Influence of Thermal Aging on the Microstructure and Mechanical Behavior of Dual-Phase, Precipitation-Hardened, Powder Metallurgy Stainless Steels

J.L. STEWART, J.J. WILLIAMS, and N. CHAWLA

The effects of thermal aging on the microstructure and mechanical behavior of dual-phase, precipitation-hardened, powder metallurgy (PM) stainless steels of varying ferrite–martensite content were examined. Quantitative analyses of the inherent porosity and phase fractions were conducted on the steels, and no significant differences were noted with respect to aging temperature. Tensile strength, yield strength, and elongation to fracture all increased with increasing aging temperature reaching maxima at 811 K (538 °C) in most cases. Increased strength and decreased ductility were observed in steels of higher martensite content. Nanoindentation of the individual microconstituents was employed to obtain a fundamental understanding of the strengthening contributions. Both the ferrite and martensite nanohardness values increased with aging temperature and exhibited similar maxima to the bulk tensile properties.

DOI: 10.1007/s11661-011-0844-3

I. INTRODUCTION

POWDER metallurgy (PM) offers many advantages including applicability to a wide variety of alloy systems, production of complex shapes, part-to-part uniformity, long-term performance reliability, minimal scrap loss, and cost effectiveness.[1] Similar to wrought counterparts, PM parts can be produced with a wide variety of microstructures to tailor mechanical behavior. They may also be heat-treated for increased strength and/or wear resistance. Early onset of plasticity and localization of strain takes place in these materials, however, as a result of reduction of the load-bearing, cross-sectional area,[2] the stress concentration effect of angular pores,[3] the potential for microcrack initiation at pores,[4–6] and the inherent inhomogeneity of pore distribution.[6–8] All of these factors are detrimental to the mechanical properties of porous steels.

The increasing demand for high-strength PM steels has led to the development of dual phase stainless steels.[9] The dual-phase steel microstructure consists of both martensite and ferrite microconstituents and is achieved through the use of austenite and ferrite stabilizers in the alloy coupled with specific processing conditions. In addition, a low carbon concentration in the alloy is necessary to coincide with the two-phase austenite-ferrite region of the Fe-C phase diagram. At higher temperatures, the steel is composed of ferrite and austenite, but upon cooling, the austenite converts to martensite and the dual-phase ferrite–martensite microstructure is achieved. This transformation is known to cause high dislocation density in ferrite near martensite-ferrite interfaces[10,11] and high residual stresses,[11–13] both of which affect the steel's mechanical behavior.

Because of the complex microstructures and mechanisms involved, dual-phase steels are known to exhibit continuous yielding behavior (*i.e.*, no defined yield point), high work hardening rate, low yield strength, and high ultimate tensile strength.[14] Dual-phase steels also benefit from their composite microstructure in that that martensite imparts strength while ferrite imparts ductility. Furthermore, the high strength of these steels results from grain boundary strengthening, through impedance of dislocation motion by grain boundaries, and is increased by the presence of grain boundaries between similar and dissimilar phases.[9] The mechanical properties of dual-phase steels and their microconstituents are also dependent on alloy and phase chemistry, thermal processing, phase fraction and size, internal stresses, and precipitate content, to name a few.[14]

The mechanical properties of dual-phase steels may be tuned by adjusting the volume fractions of the microconstituents. Many authors have studied the effect of increasing the martensite content on the mechanical behavior and have found that strength increases linearly with increasing martensite volume fraction in accordance with the rule of mixtures.[13,15–20] By conventional composite strengthening, as the fraction of the harder phase, in this case, the martensite is increased, the strength of the composite is increased. Somewhat contradictory results have been obtained in which the strength of the composite increased linearly up to a

J.L. STEWART, formerly Graduate Research Assistant, Materials Science and Engineering Program, Arizona State University, Tempe, AZ 85297-6106, is now Engineer, Intel Corporation, Chandler, AZ 85226. J.J. WILLIAMS, Research Scientist, is with the Materials Science and Engineering Program, Arizona State University. N. CHAWLA, Professor, is with the Materials Science and Engineering and Mechanical Engineering Programs, Arizona State University, 501 E. Tyler Hall, ECG 303, Tempe, AZ 85287-6106. Contact e-mail: nchawla@asu.edu
Manuscript submitted April 8, 2011.
Article published online August 9, 2011

martensite volume fraction of approximately 55 pct, after which the strength gradually decreased.[21] This behavior was attributed to a decrease in strength of the martensite resulting from lower local carbon concentration in martensite at higher martensite volume fraction. The decreased carbon content allows for easier dislocation motion and, hence, lower strength. Refinements in the microstructure, such as grain size and shape,[13,17–19,22] and martensite continuity[23] have also been shown to influence the strength of the steel, and thus phase fraction is not the sole microstructural determinant for mechanical behavior.

The technique of thermal aging is often employed to alter the mechanical properties of ferritic and/or martensitic steels. In traditional martensite-containing steels, strength generally decreases while ductility increases with increasing thermal exposure caused by tempering of the martensite. During this process, carbon diffuses out of the martensite and the tetragonal distortion of the phase is reduced, resulting in decreased residual stresses and strength of the steel composite. However, by introducing precipitation hardening elements such as copper or aluminum, dual-phase steels may be, instead, strengthened through thermal exposure.[9,24–28] First, the steel is heated to a high temperature such that diffusion of the alloying elements occurs and a supersaturated solution is formed. Second, the steel is quenched and then heated to intermediate temperatures at which the supersaturated solution decomposes and precipitates are formed that may impede dislocation motion through Orowan bowing[29] and strengthen the material. A balance of strength and ductility may thus be achieved through precipitation hardening and tempering of martensite, respectively.

One of the challenges in quantifying the composite behavior of dual-phase steels is the difficulty, to date, of investigating the properties of the individual martensite and ferrite microconstituents in dual-phase steels. In this study, we have used nanoindentation to probe the local mechanical properties of the steels' microconstituents to better understand the composite behavior. This technique is particularly valuable in dual-phase steels because of the capability of indenting individual phases. Previous studies have used nanoindentation to examine the effects of grain size,[30–33] grain boundary strengthening,[32,34–36] indentation-size–dependent strengthening,[30] carbon concentration,[27,36] thermal aging,[27,34,37–40] and precipitation hardening[29] on the mechanical properties of ferritic and/or martensitic steels. To date, very few nanoindentation studies[30,39,40] have been conducted on dual-phase steels, and to our knowledge, none have related these data to bulk tensile test results. Furthermore, the effect of precipitation hardening from copper in dual-phase steels has previously not been explored with nanoindentation.

In this study, we have examined the mechanical behavior and microstructures of dual-phase, precipitation-hardened PM stainless steels, previously developed by Schade *et al.*,[9] of varying martensite/ferrite phase fraction and aging conditions. Nanoindentation of the microconstituents was conducted to gain a deeper understanding of the mechanical properties of the bulk steels and the effects of thermal aging and precipitation hardening on the evolution of mechanical properties.

II. MATERIALS AND EXPERIMENTAL PROCEDURE

The specimens used in this study were sintered by the Hoeganaes Corporation. The nominal composition of the dual-phase, precipitation-hardened (DPPH) steel alloy is shown in Table I and includes a low carbon concentration (0.013 pct) and the presence of ferrite stabilizers (chromium, silicon, and molybdenum) and austenite stabilizers (nickel and copper) to achieve the dual-phase steel microstructure. The powders were mixed with 0.75 w/o of an organic binder (Acrawax C, Promaplast, Mexico) and compacted at 386 MPa into standard rectangular with gage and total lengths of approximately 38 mm and 86 mm, respectively. The samples were then sintered for 30 minutes at 1533 K (1260 °C) in hydrogen to a density of 6.60 g/cm^3. After cooling, the specimens were aged in 100 pct nitrogen for 1 hour at temperatures ranging from 644 K to 866 K (371 °C to 593 °C) and were cooled to room temperature. Five specimens at each of six aging temperatures were obtained. Five as sintered specimens were also retained. This group of samples is designated as low martensite (LM) because of its lower martensite content. The same steel composition and processing conditions were used to produce another set of specimens with a faster cooling rate to produce a higher martensite content. This group of samples is designated as high martensite (HM) because of its higher martensite content.

In both the LM and HM groups, specimens from four aging temperatures, as-sintered, 700 K, 811 K, and 866 K (427 °C, 538 °C, and 593 °C) were cross-sectioned and polished to a final finish of 0.05-μm silica. Porosity was characterized at three regions in each sample using optical microscopy followed by image analysis (ImageJ, Bethesda, MD). Kalling's Reagent #1 (1.5 g $CuCl_2$, 33 mL HCl, 33 mL ethanol, 33 mL water) was found to be the most effective etchant in distinguishing ferrite and martensite for this material. The specimens were etched by swabbing with the etchant for 4 minutes immediately after final polishing. This etchant colors the ferrite phase and etches the martensite.[41] Three microstructurally representative regions of each specimen were imaged using optical microscopy, and phase fractions were determined by manually shading the ferritic regions. Image processing by segmentation of the shaded images yielded the ferrite fraction. The martensite fraction was calculated by subtracting the ferrite fraction from the total area excluding the porous regions.

Table I. Nominal Powder Composition of 1 pct Cu DPPH Alloy (w/o)

C	P	Si	Cr	Ni	Cu	Mn	Mo	Fe
0.013	0.012	0.83	12.11	1.06	0.99	0.07	0.38	Balance

To obtain the local mechanical properties of the microstructure, nanoindentation (Nanoindenter XP-II; Agilent, Santa Clara, CA) was conducted on the ferrite and martensite phases of the LM and HM in as-sintered and aged steel specimens. A continuous stiffness measurement (CSM) technique was used in all experiments.[42] This technique consists of applying a small harmonic, high-frequency amplitude during indentation loading, and measuring the contact stiffness of the sample from the displacement response at the excitation frequency. The Young's modulus of the material is then derived from the contact stiffness. The main advantage of the CSM technique is that the modulus and/or hardness can be evaluated as a function of indentation depth. Indentation was conducted with a three-sided pyramid Berkovich diamond indenter on the etched specimens. Calibration for load and hardness was performed on fused silica. Indentation experiments were conducted under displacement control at a displacement rate of 50 nm/s to an indentation depth of approximately 1000 nm. The hardness and Young's modulus were averaged over a depth range of 600 to 950 nm. Within this range, both the hardness and modulus curves were constant.

All tensile rupture specimens were compacted into a dogbone geometry with an approximate gage length of 38 mm and a total length of 86 mm. Tensile testing for the LM specimens was conducted at a nominal displacement rate of 0.01–0.02 mm/s. The fracture surfaces were examined by scanning electron microscopy (SEM) using a field emission scanning electron microscope (Hitachi S-4700; Hitachi High Technologies America, Inc., Pleasanton, CA).

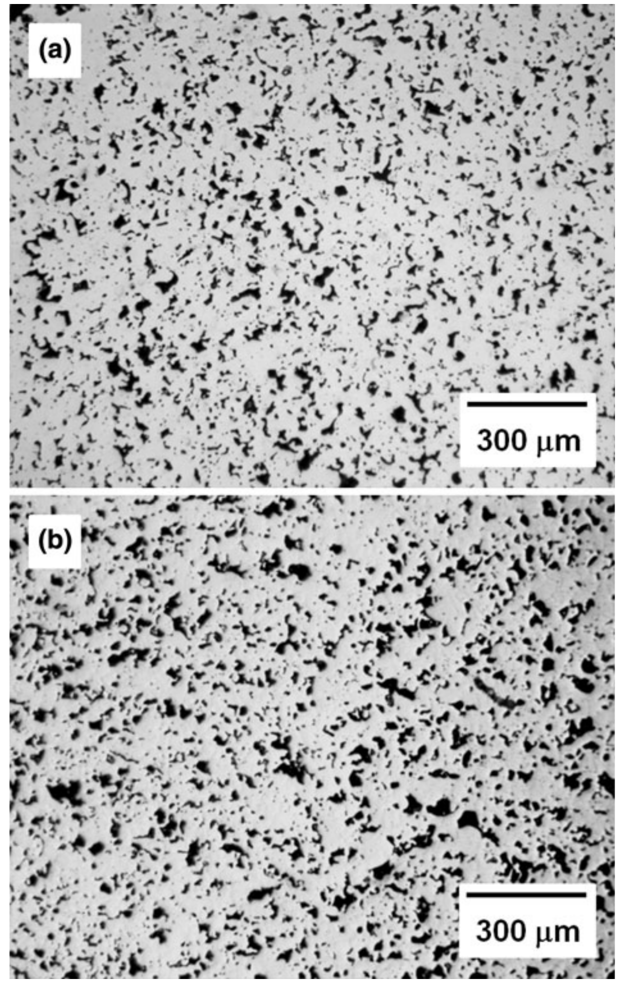

Fig. 1—Optical micrographs of (*a*) low martensite (LM) and (*b*) high martensite (HM) as-sintered specimens showing slightly higher porosity for the high martensite group.

III. RESULTS AND DISCUSSION

A. *Microstructural Characterization*

Representative optical micrographs of the porosity in LM and HM steels are shown in Figure 1. Porosity was quantified for specimens processed at the four aging temperatures previously discussed [as sintered, 700 K, 811 K, and 866 K (427 °C, 538 °C, and 593 °C)]. As Table II shows, the average porosities of the LM and HM samples were 24.2 pct and 27.1 pct, respectively. Thus, HM samples exhibited slightly higher porosity than the LM samples. The porosities do not vary significantly between aging temperatures (Table II). The tortuous nature and size of the pores is consistent between the two specimen groups, indicating similar pore geometry effects on the tensile behavior.

Table II. Porosity with Respect to Aging Temperature

Aging Temperature	LM Porosity	HM Porosity
As Sintered	24.3 ± 0.4 pct	26.6 ± 0.8 pct
700 K (427 °C)	24.2 ± 0.9 pct	27.9 ± 0.7 pct
811 K (538 °C)	24.7 ± 0.9 pct	27.3 ± 0.4 pct
866 K (593 °C)	23.6 ± 1.1 pct	26.6 ± 0.6 pct

Porosity significantly affects the mechanical behavior of steel in two ways. First, the porous areas reduce the load-bearing cross-sectional area of the tensile specimens, thus weakening them to applied loads.[2] Second, irregularly shaped pores act as stress concentrators leading to earlier onset of plasticity and localization of strain.[3] Porosity may also affect the local cooling rates of the material leading to differences in microstructure and mechanical behavior. The small difference in porosity of the LM and HM specimens may not be significant enough to cause the observed large microstructural variations. These are likely a function of the applied macroscopic cooling rate.

The high porosity content of the examined specimens indicates further influence on the steel's properties. Chawla and Deng observed that as density decreased, both the size and the irregularity of the pores increased.[43] Furthermore, at lower densities, the pores were more clustered and distributed along interstices between particles. These observations have two effects. First, irregular pore shape causes a high-stress concentration at pores that results in localized slip leading to crack initiation.[4,44] This is expected to increase with the increasing hardness of the matrix material. Second, clustering of the pores is representative of inhomogeneous distribution of pores in the material and results in areas of higher than average porosity. Fracture may then occur preferentially in these areas by crack propagation and/or void coalescence between closely neighboring pores. Furthermore, plasticity has been shown to initiate at pore clusters as a result of the higher localized stress intensity associated with these defects.[6–8]

The microstructure was studied further by etching the polished surfaces with Kalling's Reagent #1. As shown in Figure 2, optical microscopy of the etched specimens showed dual-phase microstructures containing both ferrite and martensite for both the LM and HM specimens. This microstructure is achieved through the use of specific alloying elements and processing conditions. The nominal steel composition previously presented indicates the presence of ferrite stabilizers (chromium, silicon, and molybdenum) and austenite stabilizers (nickel and copper) in the alloy. These stabilizers alter the ferrite–austenite region on the Fe-C phase diagram and support the development of the dual-phase microstructure. Also, at a sintering temperature of 1533 K (1260 °C), the alloy is in the two-phase ferrite–austenite region as a result of the low carbon concentration of the steel. Upon rapid cooling, the austenite in the steel transforms to martensite. It is not uncommon for austenite to be retained in the structure upon cooling. However, in low carbon steels, such as that studied here, the amount of retained austenite has been shown to be near zero after quenching as a result of a martensite finish temperature, M_f, above room temperature.[45] Austenite was not observed in the LM and HM micrographs.

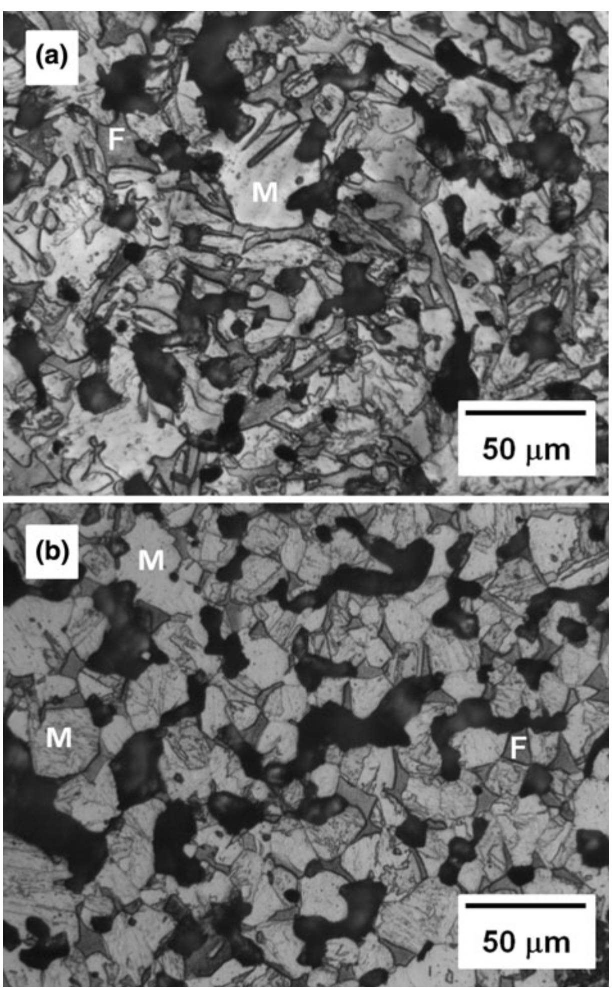

Fig. 2—Optical micrographs of (*a*) low martensite (LM) and (*b*) high martensite (HM) specimens etched with Kalling's Reagent No. 1. Ferrite and martensite are labeled with F and M, respectively.

The LM specimens exhibited ferrite and martensite phase fractions of 29 pct and 81 pct of the fully dense material, respectively. Significantly lower ferrite and higher martensite fractions of 9 pct and 92 pct, respectively, were observed in the HM specimens. The sample naming conventions of LM and HM were derived from these microstructures as a result of the lower and higher martensite fractions between the two groups. Furthermore, the phase fractions were similar for all aging temperatures within the LM and HM groups, and optical microscopy showed no significant microstructural differences between the as-sintered and aged specimens. This finding is consistent with previous studies of high-strength, low-alloy steel subjected to thermal aging.[26] It should be noted that although the phase fractions do not seem to change with aging temperature, it is possible that local diffusion and relief of residual stresses may be taking place, so that the local mechanical properties might be changing with aging temperature. Precipitates are also presumed to form upon aging but are not detectable by optical microscopy because of its limited resolution. Previous studies showed very small copper precipitates, approximately 10–50 nm in size, in steels of similar composition and aging conditions.[24,26]

B. *Mechanical Behavior of the Bulk Steels*

The stress-strain curves of the LM and HM specimens show continuous yielding behavior and the lack of defined yield points consistent with dual-phase steels (Figure 3). This behavior has been attributed to high mobile dislocation density in the ferrite near martensite interfaces[10,11] and high residual stresses resulting from the inherent volume expansion associated with the austenite-to-martensite transformation.[11–13] The austenite-to-martensite volume expansion has been reported to be approximately 2–4 pct but depends on the carbon concentration of the steel.[13,45] Upon loading, early plastic flow is observed as a result of the movement of these mobile dislocations at stresses much lower than required for mobility of restrained dislocations. Plastic flow continues in the ferrite as a result of its lower yield strength, and once this phase is significantly strained, martensite begins to deform and deformation continues in both phases simultaneously.

The ultimate tensile strength, yield strength, ductility, and Young's modulus of the LM and HM specimens are plotted as functions of aging temperature (Figure 4). The as-sintered conditions are represented at aging temperature zero. For both the LM and HM specimens,

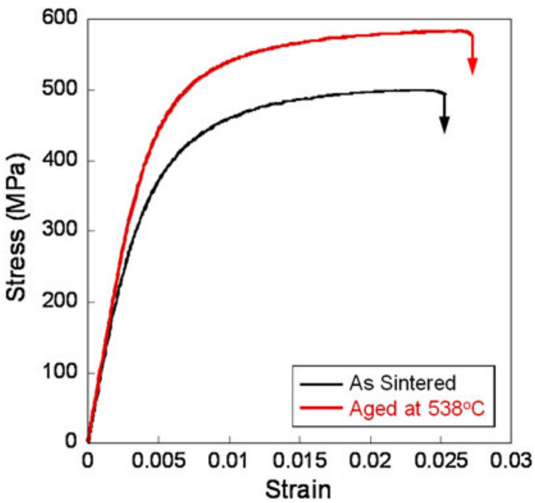

Fig. 3—Example of as-sintered and aged high martensite (HM) specimens' stress versus strain curves showing continuous yielding. Low martensite (LM) specimens also exhibit continuous yielding but are not pictured here.

the ultimate tensile strengths and yield strengths reach a maximum at an aging temperature of 811 K (538 °C). These trends presumably result from the precipitation hardening response of copper in the alloys. Up to and including 811 K (538 °C), fine precipitates form in both the ferrite and martensite resulting from aging treatments. Although these precipitates may be carbide and/or nitride based, we focus our attention on the precipitation of copper because of the low carbon and nitrogen contents of this steel. As aging temperatures are increased from the as-sintered condition to 811 K (538 °C), the copper precipitates grow in size. The dislocation mobility is impeded, and the alloy resists deformation and the ultimate tensile and yield strengths increase. At temperatures greater than 811 K (538 °C), tensile tests indicate softening occurs as a result of overaging.

Several researchers have investigated the effect of aging on copper-containing steels and have observed similar trends in strength.[9,24–28] In particular, Dhua *et al.*[26] evaluated the mechanical behavior of high-strength, low-alloy copper-bearing steels that were thermally aged and used transmission electron microscopy (TEM) to explain the strength trends. Similar to the LM and HM specimens studied here, maximum strengths were observed in specimens that were aged at 773 K (500 °C) for 1 hour. TEM showed that as the aging temperature increased, the copper precipitate size also increased from 10 to 25 nm, in the as-quenched state, to 15–30 nm at an aging temperature of 773 K (500 °C). The increase in precipitate size corresponded to the increased strength of the bulk steel. The decrease in strength after aging at 923 K (650 °C) was attributed to coarsened and slightly elongated precipitates, approximately 50 nm in maximum size, which were less effective in hindering dislocation motion. Furthermore, partial recovery of the lath martensite was observed and contributed to softening in the specimens aged at high temperatures.

Carbide precipitation has also been studied in thermally aged steel to elucidate strengthening mechanisms. Jang performed TEM experiments to determine the effect of increasing the Larson–Miller parameter (LMP) on the microstructure of 12 pct chromium ferritic steel.[34] Although LMP is generally used to quantify creep life, in Jang's study, it is simply used to describe the combined effect of time and temperature in thermal aging. As the LMP increased, the carbide precipitate size also increased and very coarse precipitates were often found in the most aged samples, the interparticle spacing increased, and the dislocation density decreased. Since all of these observations are consistent with strength degradation, it is concluded that after a certain time or temperature, overaging occurs and strengthening from precipitates becomes less effective, as in the specimens aged at 866 K (593 °C). It should be noted that in Jang's study, the aging times and temperatures were significantly higher than those used in the current study, and the results are used here to illustrate the carbide precipitation response in low carbon steels. Furthermore, it is expected that in the currently studied specimens, with their low carbon concentration, that carbide precipitation has less influence on the mechanical behavior than copper precipitation.

Increased strength with aging may also be attributed to reductions in residual internal stresses. At increased temperatures, stress relief is promoted by the tempering of martensite and carbon diffusion. The brittleness of the material is reduced, especially for steels with high martensite content.[46] This is particularly important for PM materials with highly irregular pores because stress relief reduces the notch sensitivity and improves the deformation behavior. In general, tensile strength increases with stress relief as a result of reductions in brittleness.[46] Grushko and Weiss also found this occurrence for dual-phase steels with high martensite fractions.[11] In our study, some stress relief does occur with aging as shown by increased ductility, as will be discussed later.

By simple composite strengthening theory, it is obvious that the higher strengths observed for the HM specimens are a result of their higher martensite concentrations. Intuitively, as the fraction of the stronger, harder phase increases, the strength of the composite increases. This is substantiated by previous studies that indicate that the yield and ultimate tensile strengths increase with martensite fraction.[13,15–20] Furthermore, Erdogan and Priestner[13] suggested that increases in yield strength may be a result of refinements in the microstructure. With their composite microstructure, dual-phase steels benefit from grain boundary strengthening between similar and dissimilar phases. Slight differences in the size and shape of the microconstituents therefore may affect the mechanical behavior. Consistent with these findings, Jiang *et al.* observed an increase in yield and ultimate tensile strengths with decreasing grain size in dual-phase steels.[18]

Figure 4(c) shows the superimposed plots of the elongation to fracture of the LM and HM specimens with respect to aging temperature. The HM specimens exhibit lower ductility than the LM specimens. As ferrite

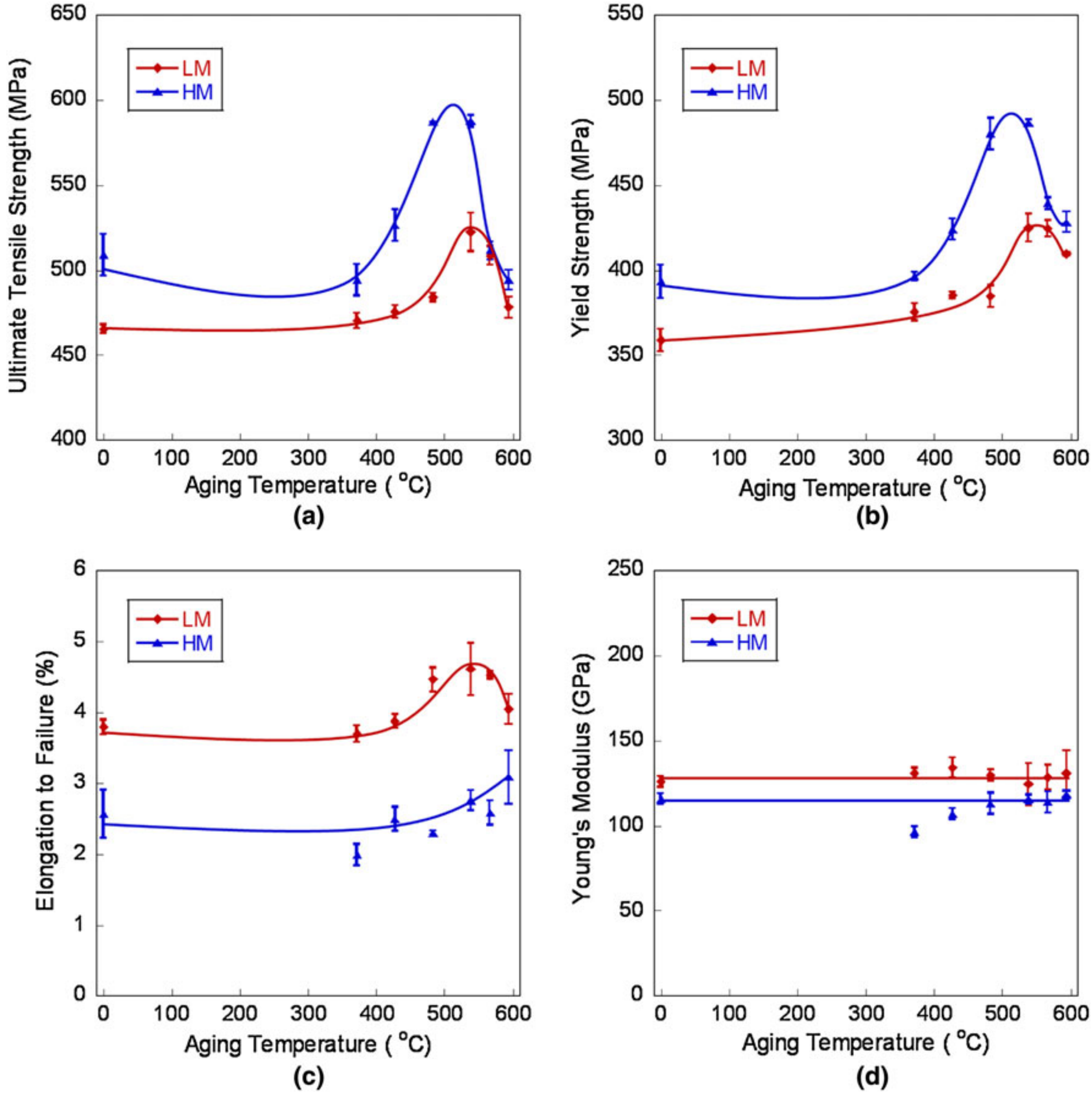

Fig. 4—Effect of thermal aging on (*a*) ultimate tensile strength, (*b*) yield strength, (*c*) elongation to failure, and (*d*) Young's modulus on low martensite (LM) and high martensite (HM) specimens. Note concurrent increases in strength and ductility with aging.

imparts ductility in dual-phase steels while martensite imparts strength, the lower ductility of the HM specimens is attributed to the higher volume fraction of martensite and hence to the lower volume fraction of ferrite in this material. Increased continuity of the martensite around the ferrite, as in the HM specimens, may also play a role in the decreased ductility.[23] The coarseness of the martensite phase also contributes to the low ductility for these specimens. Perhaps more importantly, ductility is typically inversely proportional to porosity,[47] so the slightly higher porosity of the HM specimens may be a contributing factor to their lower ductility. Higher porosity is known to be more detrimental to ductility than strength. Chawla and Deng[43] observed a significant increase in strain-to-failure with only a slight increase in density of porous sintered steels and attributed this to a narrower and more homogeneous distribution of pores. The ductility of the material may also be influenced by the size distribution, orientation, and degree of clustering of the pores because the sintered ligaments of the steel control fracture of the material.

Ductility is also shown to increase with aging, although different trends were observed for the LM and HM specimens. Similar to the yield and ultimate tensile strengths, the elongation to fracture exhibits a maximum at 811 K (538 °C) for the LM group, whereas the elongation continually increases with an increasing aging temperature for the HM group. This trend results from tempering of the martensite. Upon aging, carbon diffuses out of the martensite reducing the tetragonal shape of the martensite unit cell. Residual stresses in the microconstituents may also be reduced as a result of contraction of the martensite phase. Because of the low carbon concentration of the steels in this study, the tetragonal distortion of the martensite phase is expected to be lower than that of higher carbon steels and the effect of tempering the martensite may be less profound. Therefore, the ductility is only improved slightly with aging.

Trends in the Young's modulus versus aging temperature are considered insignificant and therefore constant. Higher moduli are observed for the LM specimens. This may be attributed to the lower porosity of the LM group because modulus increases with decreasing porosity.[48,49] As the moduli of the ferrite and martensite microconstituents are similar, the phase fractions of the LM and HM should not influence the modulus. Therefore, we may neglect the quantities of microconstituents and compare the experimental modulus data with the intrinsic porosities of the two groups. Using the model developed Ramakrishnan and Arunachalam (R-A),[50] the modulus of the fully dense material may be calculated when the modulus is known at various porosity levels. In this model, the interaction of the pores in the material is considered as the intensification of pressure on a spherical pore's surface. The Young's modulus of the material, E, is given as a function of the fraction of porosity, p[50]:

$$E = E_0 \left[\frac{(1-p)^2}{1 + \kappa_E p} \right]$$

where E_0 is the modulus of the fully dense material (which is determined by extrapolating the experimental moduli to zero porosity yielding E_0 as 254 GPa), and κ_E is a constant based on the Poisson's ratio, v_0, of the fully dense steel.

$$\kappa_E = 2 - 3v_0$$

It is assumed that the Poisson's ratio for the fully dense steel is 0.3.

Figure 5 shows a comparison between the R-A prediction and the experimental data. As observed, the experimental data and R-A prediction match reasonably well for the given range of porosity. As the model is developed on a spherical pore shape, the agreement suggests that pore shape and morphology do not significantly influence the elastic properties of the material.

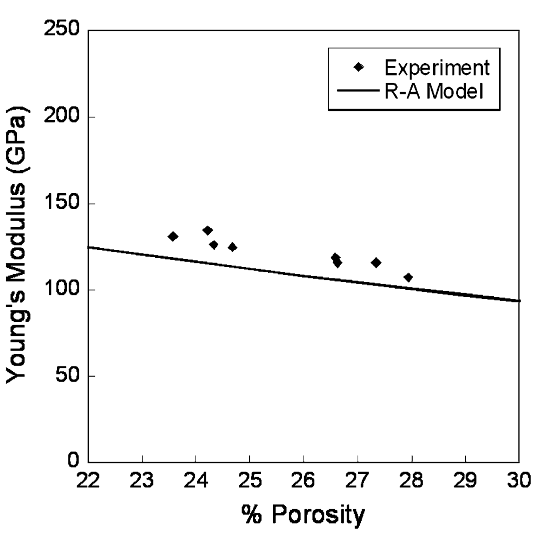

Fig. 5—Young's modulus of PM steels *vs* porosity. The R-A model predicts the experimental data well.

C. *Local Mechanical Behavior of the Microconstituents*

To quantify the mechanical properties of the local microconstituents, nanoindentation of the individual phases was performed on the LM and HM samples at the four aging conditions. Nanoindentation is a very advantageous technique, particularly for these types of microstructures, because very small areas can be probed. Use of a Vickers hardness tester might yield multiple phases being sampled and increased contributions from surrounding features. Both the ferrite and the martensite illustrated in Figure 6 were targeted with the Berkovich indenter. Attention was given to probe the centers of the grains to reduce effects from the surrounding phases. As expected, Figure 7 shows that the ferrite had lower hardness than the martensite in all samples. The HM specimens also had higher ferrite and martensite hardness values than those of the LM specimens in accordance with aging temperature, which may be attributed to different cooling rates.

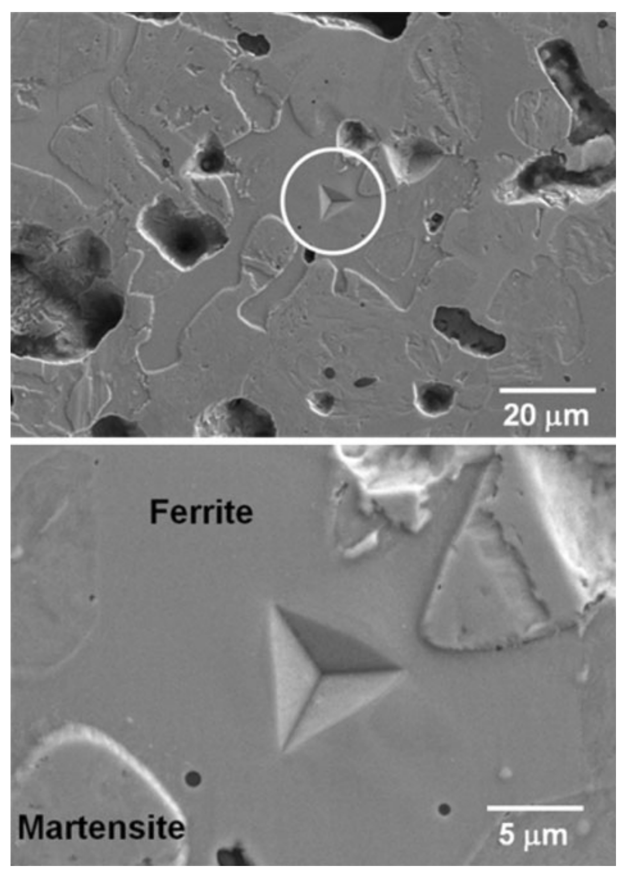

Fig. 6—Example of nanoindentation targeting individual microconstituents on etched steel surface. Ferrite and martensite are denoted by labels.

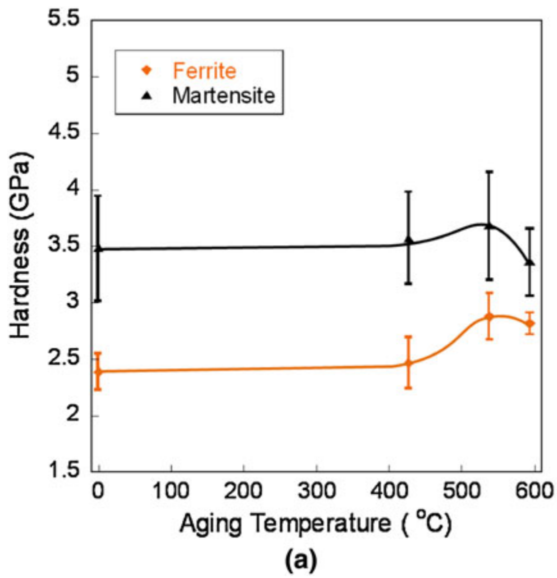

Fig. 7—Effect of thermal aging on nanohardness of ferrite and martensite in (*a*) low martensite (LM) and (*b*) high martensite (HM) specimens. Note increased hardness of both microconstituents with aging.

In the LM specimens, the hardness of the ferrite and martensite increased with aging temperature showing maxima at 811 K (538 °C). The tendency is consistent with trends observed for the yield and ultimate tensile strengths of the bulk composite during tensile testing and suggests that thermal aging influences the mechanical properties of both the ferrite and the martensite. Furthermore, these results indicate that both ferrite and martensite contribute to overall strengthening in the composite for the LM material of a relatively high ferrite phase fraction of 29 pct.

Nanoindentation results from the HM specimens exhibited the same trend in which the maximum hardness was observed at 811 K (538 °C) for martensite, but no significant maximum was observed in the hardness of the ferrite. However, aging did increase the ferrite hardness when compared with the as-sintered condition.

Although tensile testing showed strengthening behavior of the bulk LM and HM composites, nanoindentation of the ferrite and martensite constituents sheds light on the microstructural mechanism. It is shown that both ferrite and martensite are strengthened with aging and, therefore, both contribute to strengthening of the bulk LM and HM composites, although strengthening from the martensite may be dominant as a result of its much higher phase fraction. Several mechanisms are at work here. As discussed, aging causes the supersaturated solution to precipitate into small intermetallic particles. The particles strengthen the metal matrix through mechanisms such as Orowan bowing that make dislocation motion difficult.[29] As precipitates in the matrix are exceedingly smaller than the indentation volume currently used, the nanoindentation results include contributions from both the matrix and its precipitates. Increases in hardness with aging suggest that precipitation hardening occurs in both the ferrite and martensite microconstituents and the most effective precipitation response is found in specimens aged at 811 K (538 °C). At higher temperatures, overaging occurs in which precipitates have grown large enough to allow dislocations to bend and pass between adjacent particles, corresponding to a decrease in hardness. Precipitate growth also results in increased interparticle spacing, which contributes to this softening.[29] Strengthening of the ferrite phase has also previously been attributed to the grain size and solid solution hardening from the alloying elements.[16,51] The latter is more plausible in this case as a result of no apparent grain size differences between aging temperatures in the LM and HM specimens. Lastly, tempering of the martensite occurs upon aging, which relieves residual stresses, results in short-range diffusion, and contributes to enhancements in strength and ductility. At higher temperatures, temper softening may be observed as a result of rearrangement of carbon atoms and recovery of dislocation structures.[35]

Many nanoindentation studies of aged steel have been performed and have found that the hardness of martensite decreases with thermal aging as a result of degradation of the matrix strength and increased tempering of martensite.[34,35,37–40] This is in direct contradiction to the current study, which generally found increased nanohardness with thermal aging. This difference may be explained by the composition of the steels. The current specimens contain approximate 1 pct copper that, as previously explained, forms intermetallic precipitates that precipitation harden the material. In this way, this steel is unique in that two competing processes are occurring: precipitation hardening and tempering of martensite. Precipitation-hardening elements such as copper were omitted from the previously studied materials, and therefore, the materials did not benefit from strengthening induced by precipitation

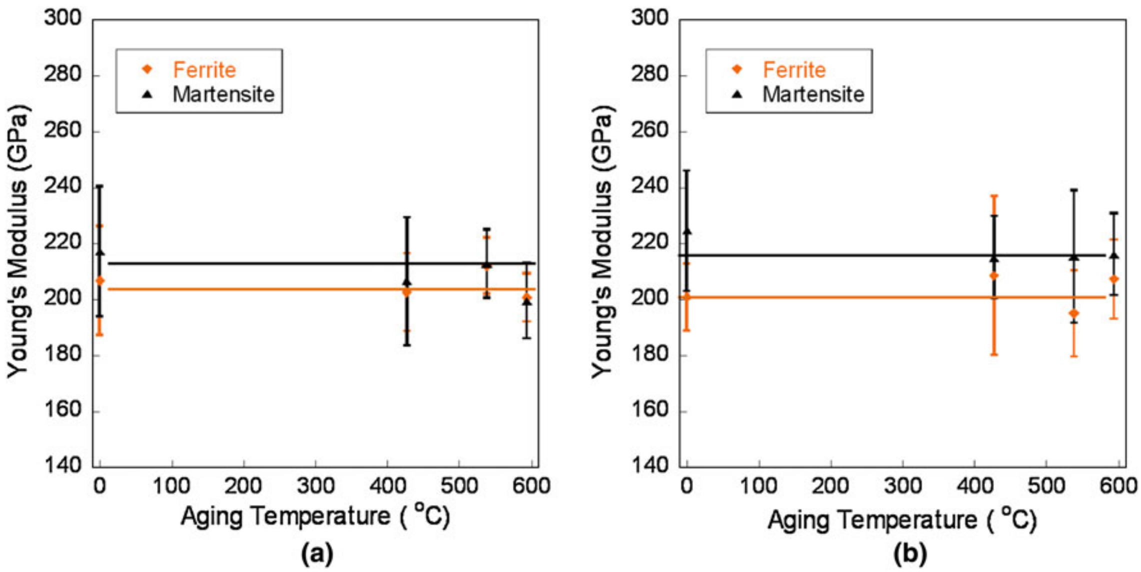

Fig. 8—Effect of thermal aging on Young's modulus of ferrite and martensite in (*a*) low martensite (LM) and (*b*) high martensite (HM) specimens showing similar values for ferrite and martensite. No significant differences in modulus are observed with aging.

hardening. Instead this response was limited to the precipitation of carbides and nitrides, of which elemental concentrations were low.

Hernandez *et al.*[39] used nanoindentation to characterize the heat-affected zone of a resistance spot-welded, wrought, dual-phase steel. They found that as the distance from the fusion zone increased, the hardness of the martensite increased, while the ferrite hardness remained relatively constant. Simulated temperature projections show an inverse logarithmic relationship between temperature and distance from the weld such that as the distance increases, the thermal exposure decreases. These results are consistent with the aforementioned studies that show decreased hardness with increased temperature. The decreased nanohardness of martensite was attributed to increased tempering as a result of the observations of more broken martensitic microstructures with the presence of submicron particles resulting from the nucleation and growth of carbides. As these carbides form, the remaining martensitic matrix is depleted of carbon and the hardness decreases. In the current study, although the carbon content is similar, this tempered appearance of martensite is not immediately apparent from optical micrographs. Hernandez *et al.* also found that the mechanical behavior of ferrite remained relatively constant with only a slight decrease in nanohardness with increased thermal exposure, which is in contrast with the currently studied specimens that showed increased nanohardness with temperature. This may be a result of differences in the compositions of the steels since Hernandez *et al.*'s steel did not contain considerable amounts of solid solution hardening elements such as silicon, which promotes hardness in ferrite.[16,51] Furthermore, this alloy did not include copper or other precipitation-hardening elements, and therefore, neither the martensite nor the ferrite benefited from the precipitation-hardening response observed in the current specimens.

As expected, the Young's moduli for the ferrite and martensite were similar over the various aging temperatures (Figure 8), and the LM and HM specimens exhibited similar moduli. As previously explained, the bulk material's modulus from tensile testing is dependent upon porosity. That is, as the porosity increases, the modulus decreases. This is not a factor in the nanoindentation modulus experiments because the small areas that were probed by the indenter were free from voids and thus considered fully dense.

D. *Fractographic Analysis*

Figure 9 shows representative scanning electron micrographs of the fractured surfaces of the as-sintered and aged at 811 K (538 °C) LM and HM specimens. Micrographs of the fracture surfaces of the tensile specimens revealed evidence of ductile rupture in the form of void nucleation and growth at second-phase particles or microstructural interfaces. Spherical inclusions of various sizes were noted in the dimples and identified as silica through energy-dispersive x-ray spectroscopy (EDS). Some elongated inclusions were also observed, suggesting partial coherency of the particles with the steel matrix. Silicon is commonly used in steel to achieve solid solution hardening[16] and to promote carbon migration from ferrite to austenite,[52] which transforms to martensite upon cooling. The evidence of silica particulates on the fracture surface indicates that both the LM and HM materials are strengthened by solid solution hardening. Efforts were taken to characterize the size distribution of the silica inclusions, but no significant trends were observed. Adequate analysis would require significant inclusion populations. Minimal areas of cleavage were also detected, but the primary rupture was ductile in nature for the as-sintered and aged specimens. Ductile rupture is expected in the ferrite phase because of its low hardness and superior

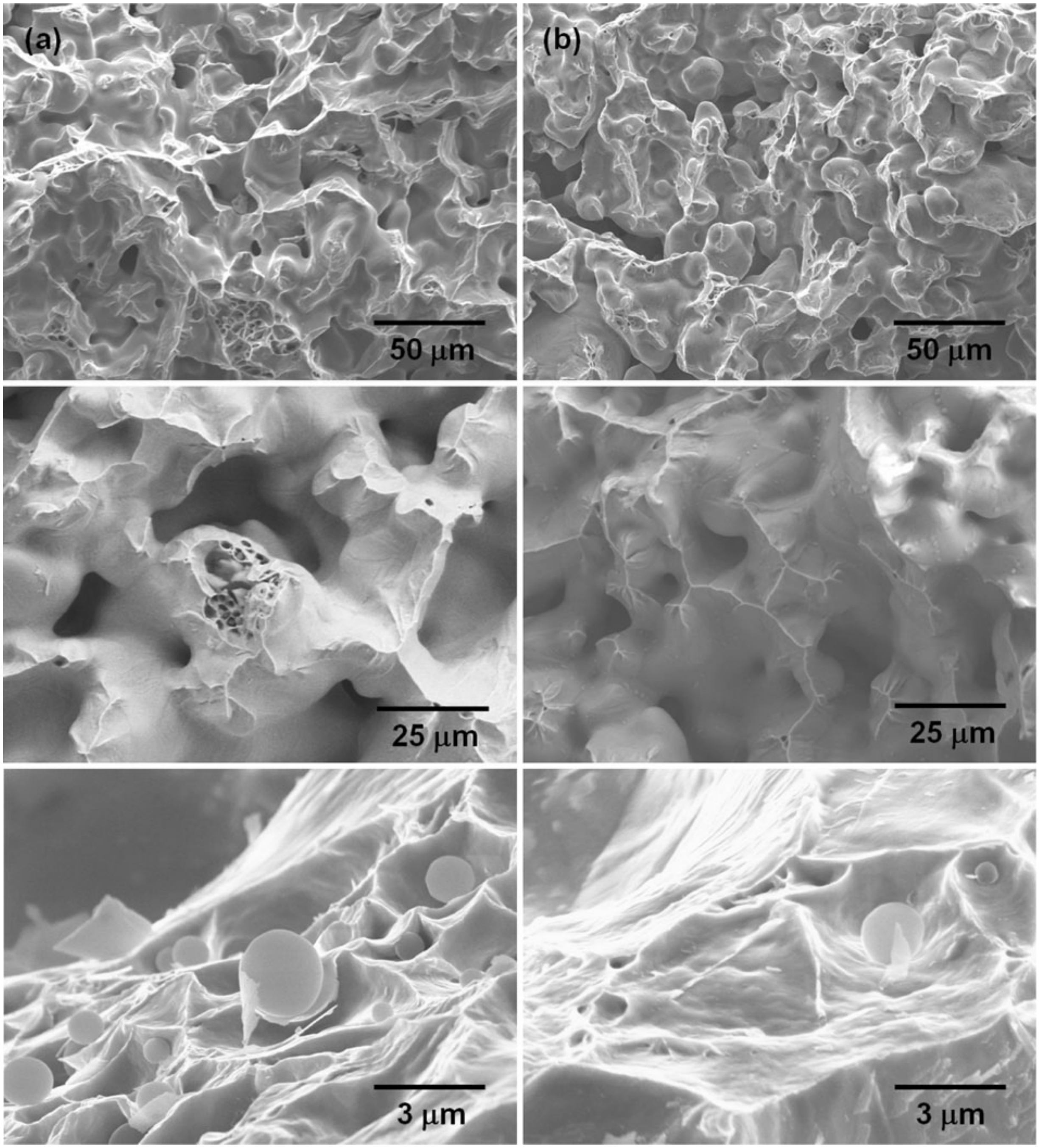

Fig. 9—Fracture surfaces of (*a*) low martensite (LM) and (*b*) high martensite (HM) specimens showing ductile rupture in the form of void nucleation and growth at second-phase silica particles and microstructural interfaces. Internal necking of the interpore matrix is observed. The micrographs are shown with increasing magnification from top to bottom.

ductility. As a result of the low carbon content of these steels and tempering from aging, it is reasonable to anticipate ductile rupture in the martensite as well. In fact, plastic deformation of martensite has been observed in previous studies of low-carbon, dual-phase steels of moderate martensite content of greater than 41 pct.[20,53] Both the LM and HM specimens have martensite volume fractions higher than this amount, so martensite plasticity is expected in all of the specimens examined here. Furthermore, no apparent differences were noted on the fracture surfaces of the LM and HM specimens. Based on the factors examined in this study, the fractographic analyses suggest that an increased martensite concentration does not affect the macroscopic ductile fracture of these alloys.

In PM materials, fracture is primarily controlled by porosity as a result of reduced load-bearing cross-sectional area and the stress concentration effect of irregularly shaped pores. When the material is plastically strained, internal necking of the interpore matrix occurs and pores grow. The area fraction of porosity, as observed in planar projections of the fracture surface, increases because of strain-induced pore growth in porous materials, thus reducing the effective load-bearing cross-sectional area.[2] Furthermore, because pores are randomly spaced, areas of higher than average porosity may exist and cause shear localization in the matrix. Preferential fracture will then occur on shorter interligament paths. Depending on the pore shape irregularity and matrix properties, microcracks may also initiate at pores[4] and propagate into the matrix by either cleavage or ductile deformation until they reach an obstacle, another microcrack, or a free surface such as another pore.

Fracture mechanisms similar to those of wrought materials may also be considered in the dense interpore matrix of sintered materials. Many studies have examined the strain distribution between phases in dual-phase steels to elucidate the damage mechanism.[54–58] Chawla *et al*.[54] found that in dual-phase steels consisting primarily of ferrite and martensite microconstituent, fracture occurs preferentially at ferrite–martensite interfaces oriented perpendicularly to the loading axis. They also found that these interfaces have larger discontinuities in mechanical properties than ferrite-inclusion interfaces. Furthermore, microvoids still form at inclusions but later than those formed at the microconstituent interfaces. In agreement with Chawla, Shen *et al*.[55] observed that shearing occurs at the martensite–ferrite interfaces and strain is transferred from the ferrite to the martensite only after the ferrite is significantly strained. In a study of dual-phase steels intercritically annealed at varying temperatures, Ray also found decohesion at the ferrite–martensite interfaces but also observed fracture in the martensite, crack formation in the ferrite adjacent to sharp martensite corners, and decohesion around inclusions and concluded that no single fracture mechanism exists for dual-phase steels.[59] It should be noted that these materials were not subjected to thermal aging, and thus, the martensite was untempered. In the current study, brittle fracture of the martensite is not expected because of its tempered microstructure and improved ductility. The tempering may also increase the probability of ductile deformation in the martensite as well as in the ferrite.

IV. CONCLUSIONS

In this study, we examined the microstructure and mechanical behavior of a PM, dual-phase, precipitation-hardened stainless steel and drew the following conclusions:

1. Higher porosity and volume fraction of martensite were observed for the HM specimens compared with the LM specimens. No significant microstructural differences were noted with aging in any specimens.
2. The HM specimens exhibited higher ultimate tensile strength and yield strength as a result of increased composite strengthening owing to their increased martensite volume fraction. The HM specimens exhibited lower ductility because of the lower ferrite fraction, increased continuity of the martensite around the ferrite, and higher porosity.
3. The yield and ultimate tensile strengths also increased with increasing aging temperature reaching a maximum at 811 K (538 °C). This behavior is attributed to precipitation hardening from the presence of copper and stress relief from carbon diffusion and tempering of the martensite. At higher temperatures, overaging occurred in which precipitates coarsen and the strength decreases. The ductility also increased slightly with aging as a result of tempering of the martensite.
4. The Young's modulus of the HM specimens was lower than the LM specimens as a result of increased porosity. The Young's modulus of the fully dense material, which was determined from extrapolation of the experimental data, agreed very well with the theoretical value obtained using the R-A model,[50] suggesting little influence of pore shape and morphology on the elastic properties of the material.
5. Nanoindentation of the microconstituents showed higher hardness for martensite than for ferrite in all cases, owing to martensite's high dislocation density and tetragonal lattice supersaturated with carbon. The HM specimens had higher hardness values for both the martensite and the ferrite.
6. Both the martensite and ferrite hardness values were shown to increase with increased aging temperature and in many cases showed peak hardness at 811 K (538 °C), which is consistent with bulk tensile test results. Because precipitates in the matrix are exceedingly smaller than the indentation volume currently used, the nanoindentation results include contributions from both the matrix and its precipitates and show that both the ferrite and the martensite benefit from precipitation hardening. Therefore, both microconstituents contribute to the increased strength of the bulk steel with aging as observed in tensile tests.
7. Micrographs of the fracture surfaces of the tensile specimens revealed evidence of ductile rupture in the form of void nucleation and growth at second-phase particles or microstructural interfaces.

ACKNOWLEDGMENTS

The authors acknowledge the Hoeganaes Corporation for providing the materials and financial support for this research. We would also like to thank C. Schade and T. Murphy for stimulating discussions related to this work.

REFERENCES

1. Introducing Powder Metallurgy (PM): www.mpif.org.
2. R.J. Boucier, D.A. Koss, R.E. Smelser, and O Richmond: *Acta Metall.*, 1986, vol. 34 (12), pp. 2443–53.

3. G Straffelini: *Powder Metall.*, 2005, vol. 48 (2), pp. 189–92.
4. J. Holmes and R.A. Queeney: *Powder Metall.*, 1985, vol. 28, p. 231.
5. H.E. Exner and D. Pohl: *Powder Metall.*, 1978, vol. 10, pp. 193–96.
6. X. Deng, G.B. Piotrowski, J.J. Williams, and N. Chawla: *Int. J. Fatigue*, 2005, vol. 27, pp. 1233–43.
7. A. Hadrboletz and B. Weiss: *Int. Mater. Rev.*, 1997, vol. 42, pp. 1–44.
8. S.J. Polasik, J.J. Williams, and N. Chawla: *Metall. Mater. Trans. A*, 2002, vol. 33A, p. 73.
9. C.T. Schade, T.F. Murphy, A. Lawley, and R Doherty: *Int. J. Powder. Metall.*, 2009, vol. 45 (1), pp. 38–46.
10. H.J. Klaar, I.A. El-Sesy, and A.H.A. Hussein: *Steel Res.*, 1990, vol. 61 (2), pp. 85–92.
11. B. Grushko and B.Z. Weiss: *Scripta Metall.*, 1989, vol. 23, pp. 865–70.
12. D.K. Matlock, G. Krauss, L. Ramos, and G.S. Huppi: *Structure and Properties of Dual-Phase Steels*, American Institute of Mining, Metallurgical, and Petroleum Engineers, Littleton, CO, 1979, pp. 62–90.
13. M. Erdogan and R. Priestner: *Mater. Sci. Technol.*, 1999, vol. 15, pp. 1273–84.
14. M.S. Rashid: *Ann. Rev. Mater. Sci.*, 1981, vol. 11, pp. 245–66.
15. I. Tamura, Y. Tomata, A. Okao, Y. Yamaoha, H. Ozawa, and S. Kaotoni: *Trans ISIJ*, 1973, vol. 13, pp. 283–92.
16. G.R. Speich and R.L. Miller: *Structure and Properties of Dual-Phase Steels*, American Institute of Mining, Metallurgical, and Petroleum Engineers, Littleton, CO, 1979, pp. 145–82.
17. S. Gunduz, B. Demir, and R. Kacar: *Ironmaking Steelmaking*, 2008, vol. 35 (1), pp. 63–66.
18. Z. Jiang, Z. Guan, and J. Lian: *Mater. Sci. Eng. A*, 1995, vol. 190, pp. 55–64.
19. A. Gural, S. Tekeli, and T. Ando: *J. Mater. Sci.*, 2006, vol. 41, pp. 7894–901.
20. M. Sarwar and R. Priestner: *J. Mater. Sci.*, 1996, vol. 31, pp. 2091–95.
21. A. Bag, K.K. Ray, and E.S. Dwarakadasa: *Metall. Mater. Trans. A*, 1999, vol. 30A, pp. 1193–1202.
22. P.H. Chang and A.G. Preban: *Acta Metall.*, 1985, vol. 35 (5), pp. 897–903.
23. K. Kocatepe, M. Cerah, and M. Erdogan: *J. Mater. Process. Technol.*, 2006, vol. 178, pp. 44–51.
24. S.K. Ghosh, A. Haldar, and P.P. Chattopadhyay: *J. Mater. Sci.*, 2009, vol. 44, pp. 580–90.
25. C.N. Hsaio, C.S. Chiou, and J.R. Yang: *Mater. Chem. Phys.*, 2002, vol. 74, pp. 134–42.
26. S.K. Dhua, A. Ray, and D.S. Sarma: *Mater. Sci. Eng. A*, 2001, vol. 318, pp. 197–210.
27. T. Ohmura, K. Sawada, K. Kimura, and K. Tsuzaki: *Mater. Sci. Eng. A*, 2008, vol. 489, pp. 85–92.
28. L. Pussegoda and W.R. Tyson: *Can. Metall. Q.*, 23, 1984, pp. 341–47.
29. J. Moon, S. Kim, J. Jang, J. Lee, and C. Lee: *Mater. Sci. Eng. A*, 2008, vol. 487, pp. 552–57.
30. M. Delince, P.J. Jacques, and T. Pardoen: *Acta Mater.*, 2006, vol. 54, pp. 3395–404.
31. T. Ohmura, K. Tsuzaki, and S. Matsuoka: *Scripta Mater.*, 2001, vol. 45, pp. 889–94.
32. Y. Choi, W.Y. Choo, and D. Kwon: *Scripta Mater.*, 2001, vol. 45, pp. 1401–06.
33. T.H. Ahn, K.K. Um, J.K. Choi, D.H. Kim, K.H. Oh, M. Kim, and H.N. Han: *Mater. Sci. Eng. A*, 2009, vol. 523, pp. 173–77.
34. J Jang: *J. Mater. Res.*, 2007, vol. 22 (1), pp. 175–85.
35. T. Ohmura and K. Tsuzaki: *J. Phys. D: Appl. Phys.*, 2008, vol. 41, pp. 1–6.
36. T.B. Britton, D. Randman, and A.J. Wilkinson: *J. Mater. Res.*, 2009, vol. 24 (3), pp. 607–15.
37. T. Ohmura, T. Hara, and K. Tsuzaki: *Scripta Mater.*, 2003, vol. 49, pp. 1157–62.
38. T. Ohmura, K. Tsuzaki, and S. Matsuoka: *Phil. Mag. A*, 2002, vol. 82, pp. 1903–10.
39. V.H.B. Hernandez, S.K. Panda, Y. Okita, and N.Y. Zhou: *J. Mater. Sci.*, 2010, vol. 45, pp. 1638–47.
40. V.H.B. Hernandez, S.K. Panda, M.L Kuntz, and Y. Zhou: *Mater. Lett.*, 2010, vol. 64, pp. 207–10.
41. G.F. Vander Voort, G.M. Lucas, and E.P. Manilova: *Metallography and Microstructures of Stainless Steels and Maraging Steels*, ASM Handbook 9, 2004, pp. 670–700.
42. W.C. Oliver and G.M. Pharr: *J. Mater. Res.*, 1992, vol. 7, p. 1564.
43. N. Chawla and X. Deng: *Mater. Sci. Eng. A*, 2005, vol. 390, pp. 98–112.
44. K.M. Vedula and R.W. Heckel: *Modern Developments in Powder Metallurgy*, Metal Powder Industries Federation, Princeton, NJ, 1981.
45. R.E. Reed-Hill and R. Abbaschian: *Physical Metallurgy Principles*, 3rd ed., PWS Publishing Company, Boston, MA, 1994.
46. T. Marcu, A. Molinari, G. Straffelini, and S. Berg: *Int. J. Powder Metall.*, 2004, vol. 40 (3), pp. 57–64.
47. W.A. Spitzig, R.E. Smelser, and O. Richmond: *Acta Metall.*, 1988, vol. 36 (5), pp. 1201–11.
48. A. Salak: *Ferrous Powder Metallurgy*, Cambridge International Science Publishing, Cambridge, UK, 1997.
49. N. Chawla, F. Ochoa, V.V. Ganesh, and X. Deng: *J. Mater. Sci. Mater. Electron.*, 2004, vol. 15, pp. 385–88.
50. N. Ramakrishnan and V.S. Arunachalam: *J. Am. Ceram. Soc.*, 1993, vol. 76, p. 2745.
51. Q. Furnemont, M. Kempf, P.J. Jacques, M. Goken, and F. Delannay: *Mater. Sci. Eng. A*, 2002, vol. 328, pp. 26–32.
52. P. Abramowitz and R.A. Moll: *Metall. Trans.*, 1970, vol. 1, pp. 1773–75.
53. M. Mazinani and W.J. Poole: *Metall. Mater. Trans. A*, 2007, vol. 38A, pp. 328–39.
54. K.K. Chawla, P.R. Rios, and J.R.C. Guimaraes: *J. Mater. Sci. Lett.*, 1983, vol. 2, pp. 94–98.
55. H.P. Shen, T.C. Lei, and J.Z. Liu: *Mater. Sci. Technol.*, 1987, vol. 3, pp. 415–21.
56. F.M. Al-Abbasi and J.A. Nemes: *Int. J. Mech. Sci.*, 2003, vol. 45, pp. 1449–65.
57. E. Maire, O. Bouaziz, M. Di Michiel, and C. Verdu: *Acta Mater*, 2008, vol. 56, pp. 4954–64.
58. X. Sun, K.S. Choi, W.N. Liu, and M.A. Khaleel: *Int. J. Plast.*, 2009, vol. 25, pp. 1888–1909.
59. R.K. Ray: *Scripta Metall.*, 1984, vol. 18, pp. 1205–09.